AIP Journal of Applied Physics

Characteristics of atmospheric-pressure non-thermal N2 and N2/O2 gas mixture plasma jet

Dezhi Xiao, Cheng Cheng, Jie Shen, Yan Lan, Hongbing Xie, Xingsheng Shu, Yuedong Meng, Jiangang Li, and Paul K. Chu

Citation: Journal of Applied Physics **115**, 033303 (2014); doi: 10.1063/1.4862304
View online: http://dx.doi.org/10.1063/1.4862304
View Table of Contents: http://scitation.aip.org/content/aip/journal/jap/115/3?ver=pdfcov
Published by the AIP Publishing

Characteristics of atmospheric-pressure non-thermal N_2 and N_2/O_2 gas mixture plasma jet

Dezhi Xiao,[1] Cheng Cheng,[1,2,a)] Jie Shen,[1] Yan Lan,[1] Hongbing Xie,[1] Xingsheng Shu,[1] Yuedong Meng,[1] Jiangang Li,[1] and Paul K. Chu[2,a)]
[1]*Institute of Plasma Physics, Chinese Academy of Sciences, P. O. Box 1126, Hefei 230031, People's Republic of China*
[2]*Department of Physics and Materials Science, City University of Hong Kong, Tat Chee Avenue, Kowloon, Hong Kong, China*

(Received 11 September 2013; accepted 3 January 2014; published online 17 January 2014)

An atmospheric-pressure non-thermal plasma jet driven by high frequency alternating current and operating on N_2 and N_2/O_2 gas mixture is investigated. The plasma jet can reach 55 mm in length at a gas flow rate of 2500 l/h. The gas temperature at a distance of 4 mm from the nozzle is close to room temperature. Optical emission spectroscopy is employed to investigate the important plasma parameters such as the excited species, rotational temperature, vibrational temperature, and excitation temperature under different discharge conditions. The results show that the plasma source operates under non-equilibrium conditions. The absolute irradiance intensity of the vibrational band N_2(C-B) in the active region is measured. Taking into account the irradiance intensity of N_2(C-B,0-0) and N_2(B-X,0-0) as well as measured current, the electron density, which is determined by considering direct and step-wise electron impact excitation of nitrogen emission, reaches a maximum value of $5.6 \times 10^{20}/m^3$. © *2014 AIP Publishing LLC*.
[http://dx.doi.org/10.1063/1.4862304]

I. INTRODUCTION

Atmospheric-pressure non-thermal plasma sources which are typically simple and economical have undergone extensive development in recent years. Many types of atmospheric-pressure plasma jets (APPJs) based on different power sources and configurations have been reported.[1–4] APPJs are commonly used in sterilization, killing of cancer cells, air cleaning, waste water treatment, as well as materials and surface treatment,[5–11] because they generate plasmas in the open air and there is no limitation on the size of the objects to be treated. Most APPJs operate on noble gases or mixtures of noble gases with small amounts of reactive gases such as O_2, CF_4, H_2O, and so on[12–14] as the feeding gas. Replacement of the noble gases by more economical gases such as nitrogen or air can reduce the operating costs. In general, the gas temperature of the N_2 or air plasma ranges from hundreds to thousands Kelvin and the high temperature limits biomedical applications. Recently, APPJs employing N_2 or air as the working gas have been developed to overcome the problem.[15–17] Herein, we report a non-thermal plasma jet operating on N_2 or a N_2/O_2 gas mixture and its characteristics are investigated. The plasma jet can be touched with the bare hands and used in biomedical applications including inactivation of microorganisms and wound healing.

Copious quantities of reactive oxygen and nitrogen species are often generated in atmospheric pressure plasmas, especially when N_2 and N_2/O_2 are the working gas, and they are also known to play active roles in biomedical applications. The reactive species and amounts generated depend on plasma parameters, such as the rotational, vibrational, excitation temperature and electron density. Better understanding of the plasma parameters can provide insights into the roles of the active species in biomedical applications. According to some reports,[4,11,13] direct influence of the plasma produces inactivation faster than the indirect treatment. Therefore, the study on the characteristics of the active zone and afterglow of the discharge is very important.

In order to measure these parameters, optical emission spectroscopy (OES) is a widely used diagnostic tool, which imparts valuable information about the excited atomic and molecular states as well as rotational, vibrational, and electronic excitation of the plasma species. As an important parameter, the electron density is traditionally monitored by a Langmuir probe, laser heterodyne interferometry, laser Thomson scattering, and Stark broadening of different Balmer hydrogen lines.[18–23] However, the probe method is not suitable for electron density measurement at atmospheric pressure because of the limited size of the discharge. Laser heterodyne interferometry and laser Thomson scattering are rarely adopted in atmospheric pressure plasma diagnosis because they involve complicated and expensive laser systems. Stark broadening can only measure the electron density larger than $5.0 \times 10^{19}/m^3$,[24] which is limited to the weak discharge where the electron density is always smaller than the threshold value. Awakowicz *et al.*[25–27] have used experimental and theoretical diagnostic methods such as Boltzmann's equation and OES to determine the electron density and electric field. In this work, an atmospheric-pressure non-equilibrium plasma jet excited by alternating current (AC) is investigated. The electrical characteristics are monitored based on the discharge voltage and current, and the jet length is measured using a camera. We systematically study the rotational and vibrational temperature at different discharge

a)E-mail addresses: chengcheng@ipp.ac.cn and paul.chu@cityu.edu.hk

power, flow rates, oxygen percentage in nitrogen, and positions by measuring the rotational and vibrational bands of the second positive system of N_2. The rotational temperature is determined by comparing the simulated and experimental spectra. The vibrational temperature depends on the relative intensity distributions of the vibrational bands according to the Boltzmann-plot method. The excitation temperature is estimated by the ratio of the intensities of the spectral lines of Cu I based on Boltzmann's method. By monitoring the irradiance intensity spectra, the electron excitation processes are analyzed by solving Boltzmann's equation with the consideration of the plasma volume in the active region and other factors. The electron density is determined by applying the absolute intensity of N_2(C-B,0-0) at 337.1 nm and N_2^+(B-X,0-0) at 391.4 nm. The electrical model is also introduced to estimate the electron density.

II. EXPERIMENTAL APPARATUS

The atmospheric-pressure non-thermal AC plasma jet is schematically presented in Fig. 1. The outside electrode is a stainless steel cylinder with an external diameter of 14 mm and thickness of 3 mm connected to ground. A copper rod with a diameter of 2 mm is partially covered by a quartz tube to restrict the discharge to a small area. The distance between the inner electrode and outer electrode is approximately 2 mm. The AC power supply is a commercial transformer capable of continuous and tunable output voltages and frequencies. The applied voltage and discharge current of the jet are monitored on a Tektronix MSO 5104 digital oscilloscope equipped with a high voltage probe (Tektronix P6015A) and current probe (Tektronix P6021). The gas flow into the chamber from the two gas inlets and maximum flow rates of nitrogen and oxygen are 2500 l/h and 200 l/h, respectively. The volume ratio of oxygen injected into the plasma jet is designated as $O_2/(N_2+O_2)$. The plasma is generated between the two electrodes and leaves the nozzle with a diameter of 4 mm. The emission spectra are acquired *via* an optical fiber and analyzed by an AvaSpec-2048 spectrometer equipped with a holographic grating of 2400 lines/mm and a 10 μm wide slit. This spectrometer is calibrated by AvaLight-DH-CAL. With regard to the end emission spectra in Fig. 1(a), one quartz fused silica lens (50 mm in diameter and a focal length of 10 mm) is used to focus the end images onto the optical fiber. For the spatially resolved side emission spectra shown in Fig. 1(b), the optical fiber bundle is used directly to collect the light from the jet. The side emission spectra are taken along the jet 0 to 12 mm away from the exit nozzle. The images of the non-thermal plasma jet are captured by a digital camera (Canon 5D Mark II) with an exposure time of 0.04 s. The representative images of the plasma jet at a total flow rate of 1000 l/h and discharge power of 22.7 W in nitrogen are depicted in Fig. 1(c). The plasma is homogeneous and bright and its length is about 30 mm. Although the plasma is bright, the gas temperature of the plasma is not high and touchable. In order to reduce errors in the plasma parameters, several independent experiments were performed under the same conditions and the results represented the average of several independent experiments.

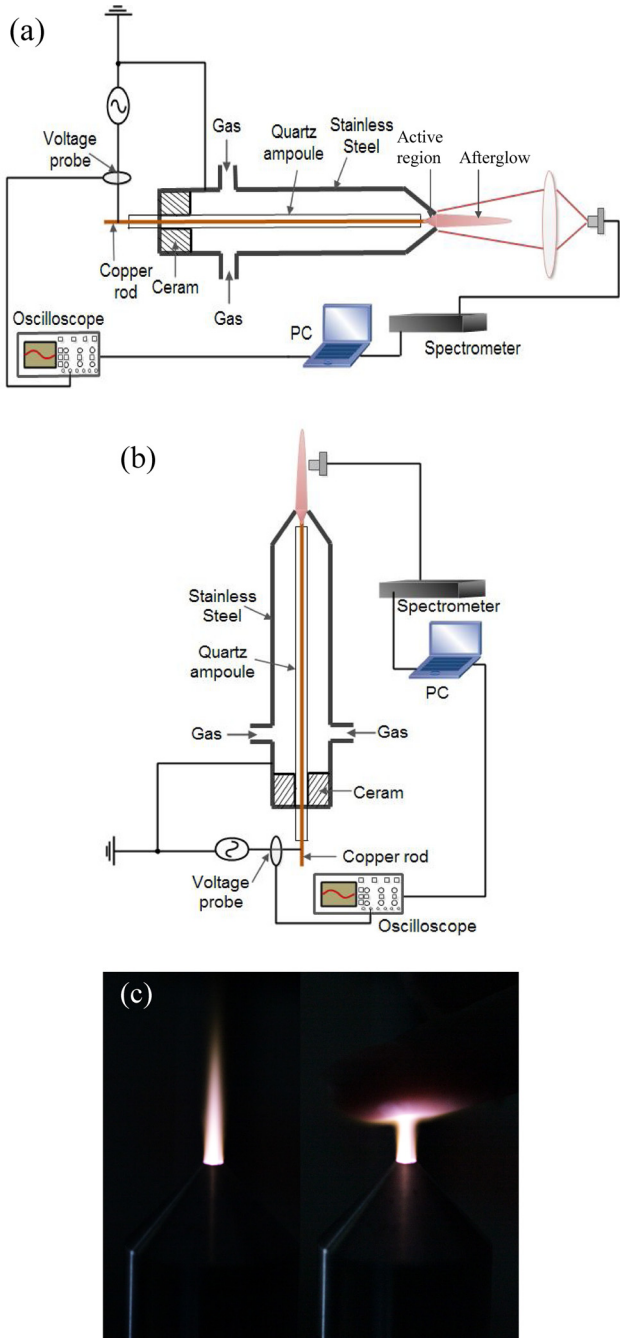

FIG. 1. (a) Experiment setup schematic—end configuration and (b) Experimental setup schematic—side configuration; (c) Image of discharge in nitrogen at discharge power of 22.7 W and flow rate of 1000 l/h.

III. RESULTS AND DISCUSSION

A. Electrical characteristics

The voltage and current waveforms obtained at a nitrogen flow rate of 1000 l/h are displayed in Fig. 2. When the voltage is high enough to ionize the working gas, voltage breakdown and pulse current occur. The peak voltage and current are approximately 3.0 kV and 4.5 A measured by the probes. The frequency of the discharge is the same as that of

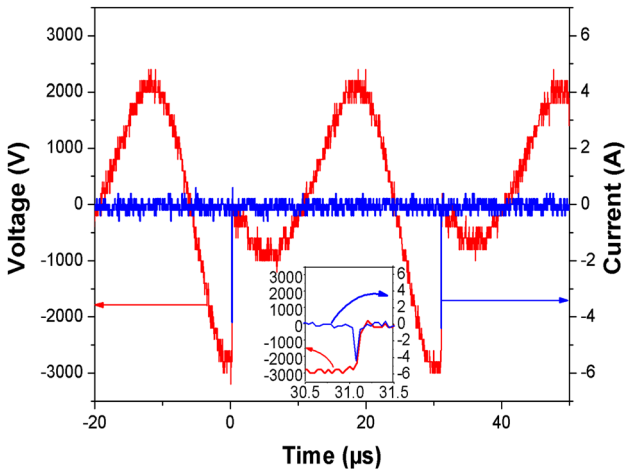

FIG. 2. Voltage and current waveforms of the discharge in nitrogen at a flow rate of 1000 l/h.

the applied voltage and the width of the current pulse is about 80 ns. The average power dissipated into the plasma is calculated by integrating the product of the discharge voltage and current over one cycle according to the following formula:

$$P = \frac{1}{T}\int_0^T U(t)I(t)dt,$$

where T is the discharge period and the average discharge power is about 18 W. Because the current pulse duration is only tens of nanoseconds (inset in Fig. 2), the dissipated power is small and for this reason, this plasma jet is different from a traditional one in which the temperature is usually too high to touch.

B. Images and jet length

The changes in the plasma jet lengths for different flow rates with different discharge power, different volume ratio of oxygen injection with different discharge power, and different discharge frequencies are shown in Figs. 3(a)–3(c), respectively. The length of the plasma jet increases with increasing discharge power regardless of changes of the other experimental conditions, but when the discharge power continues to increase (≥22.7 W), the plasma jet length does not change significantly. Fig. 3(a) shows that the plasma jet length increases with the flow rate. At a small input power (18.0 W), the plasma length is about 27 mm at a flow rate of 1250 l/h and the growth rate becomes flat despite further increase in the flow rate. The plasma length increases with the flow rate at high discharge power (≥22.7 W) and reaches 55 mm at a flow rate of 2500 l/h. As shown in Fig. 3(b), when a small amount of oxygen is introduced, the plasma length decreases with increasing oxygen concentrations. Because oxygen is an electronegative gas which attracts electrons, the discharge intensity diminishes and the plasma jet length is reduced. Fig. 3(c) shows that when the discharge frequency is varied, the jet length does not change much at a fixed discharge power of 22.7 W and flow rate of 1000 l/h. It may be because when the discharge power is fixed, the power dissipated into the plasma does not change significantly even through the discharge frequency is changed.

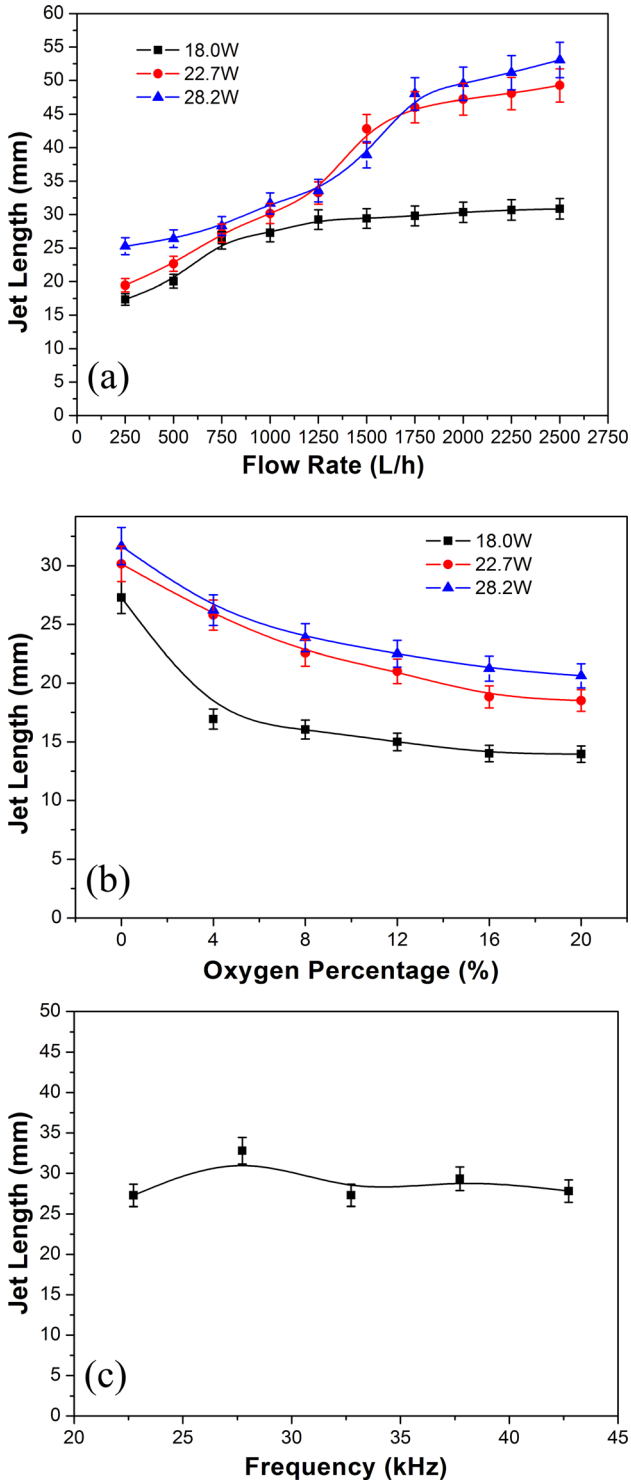

FIG. 3. Plasma jet lengths: (a) Flow rate between 250 l/h and 2500 l/h in nitrogen discharge, (b) Oxygen percentage from 0 to 20% with a flow rate of 1000 l/h, and (c) frequency from 20.73 kHz to 42.73 kHz with a flow rate of 1000 l/h and discharge power of 22.7 W.

C. Spectroscopic and temperature measurements

1. Spectra and lines identification

OES is a common technique to determine the plasma parameters, such as the excited species, rotational temperature

(T_{rot}), vibrational temperature (T_{vib}), and excitation temperature (T_{exc}). The typical survey spectra for end-on and side-on in a range of 200–900 nm in the plasma regions for N_2 discharge and $N_2/O_2(8\%)$ at a flow rate of 1000 l/h and discharge power of 22.7 W are presented in Fig. 4. The end-on emission spectra in the active region of the N_2 and N_2/O_2 (8%) discharge are shown in Figs. 4(a) and 4(b), respectively. With regard to these two discharges, the emission spectra are dominated by excited nitrogen species, for instance, N_2 second positive system in the UV region ($N_2(C^3\Pi_u - B^3\Pi_g)$), N_2^+ first negative system ($N_2^+(B^2\Sigma_u - X^2\Sigma_g)$), and N_2 fist positive system ($N_2(B^3\Pi_g - A^3\Pi_u)$). In addition, atomic nitrogen at 747, 822, and 868 nm is observed from the active region due to electron impact dissociation ($N_2 + e \rightarrow 2N + e$). These lines are identified by comparison to Refs. 15–17 and 28–30. Compared to the N_2 discharge, highly reactive atomic oxygen at 777 ($3p^5P \rightarrow 3s^5S$)[17] and 844 nm ($3p^5P \rightarrow 3s^5S$)[30] and the band of NO_γ-system at 200–300 nm ($NO(A^2\Sigma - X^2\Sigma)$)[28] are detected due to oxygen introduction into the working gas. Fig. 4(c) shows the emission spectra of N_2 discharge in the afterglow regions. A spectrum similar to that in the active region of the N_2 discharge is obtained. However, a characteristic difference in emission from atomic nitrogen is observed, suggesting that atomic nitrogen is generated and exited in the reactive region. The discharge path in the reactive region is from the top of the inner electrode to near the exit of the jet nozzle. Dissociation of molecular nitrogen requires large energy of at least 10 eV. Therefore, it is believed that the high energy electrons are generated near the exit of the jet nozzle. According to Xian's report,[31] a similar plasma in the afterglow is not driven by the electric field, and so the plasma jet outside the nozzle cannot obtain the sustained energy and energy will be lost *via* collisions. Hence, there are no emission lines of atomic nitrogen in the afterglow region. Besides the difference of atomic nitrogen in the emission spectrum, the γ-system ($NO(A^2\Sigma^2\text{-}X^2\Pi)$ transitions) in the 200–300 range is shown in Fig. 4(c) compared to Fig. 4(a). The NO_γ bands due to the emission of $NO(A^2\Sigma^2) \rightarrow NO\ (X^2\Pi)$ comes from dissociation of molecular nitrogen and oxygen in open air.

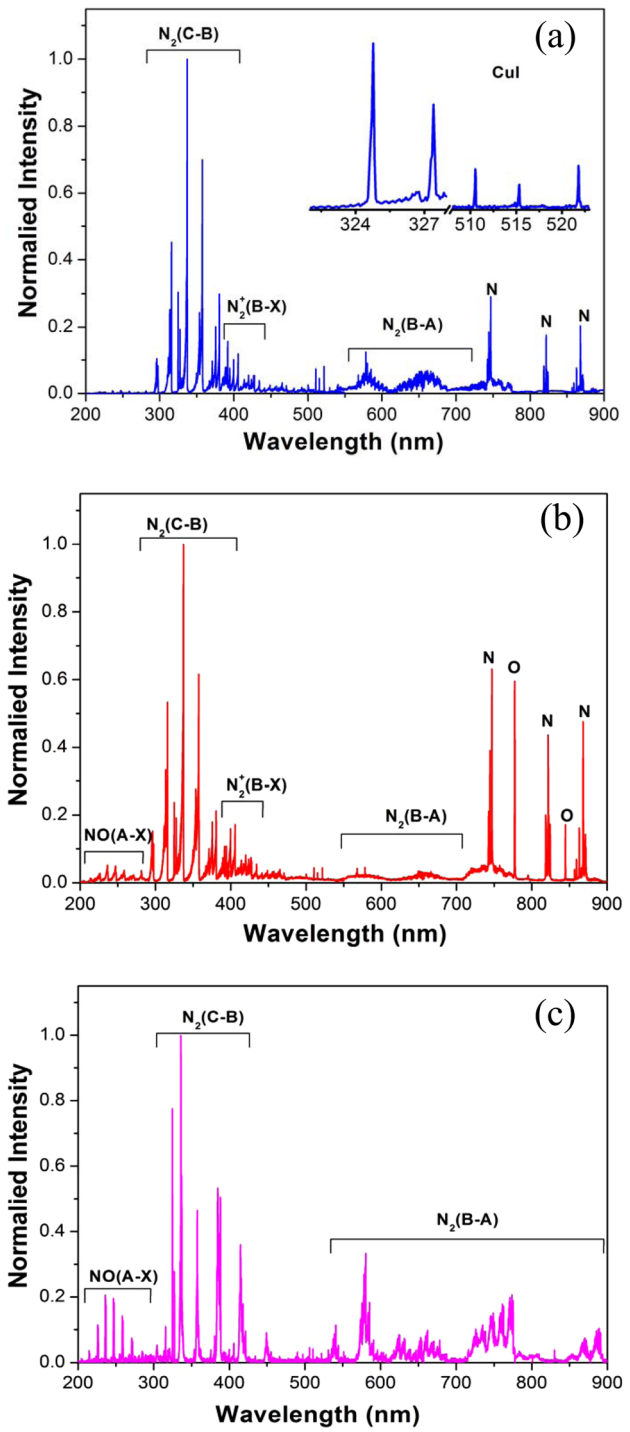

FIG. 4. Emission spectra at discharge power of 22.7 W and flow rate of 1000 l/h; (a) End measurement in nitrogen; (b) End measurement in nitrogen/oxygen; (c) Side measurement in nitrogen.

The changes in some special emission line intensities (N_2(C-B,0-0) at 337.1 nm, N_2^+(B-X,0-0) at 391.4 nm, O at 777.4 nm, and O at 844.7 nm) under some discharge conditions (discharge power and oxygen percentage) are investigated, and the results are presented in Fig. 5. As shown in Fig. 5(a), the emission intensity of the lines of N_2 (337.1 nm) and N_2^+ (391.4 nm) increases with discharge power, indicating that when the discharge power rises, more power dissipates and more N_2 molecules are excited and ionized. The emission intensity of afterglow is much weaker than that of the active region, especially the emission intensity of N_2^+ (391.4 nm). It is because the plasma can obtain much more energy in the active region. With rising oxygen percentage, the emission intensity of the lines of N_2 (337.1 nm) and N_2^+ (391.4 nm) decreases and that of O (777.4 nm) and O (844.7 nm) increases (Fig. 5(b)) in the active region. When the percentage is up to 12%, the intensity of O (777.4 nm) is larger than that of N_2 (337.1 nm). It is mainly because oxygen is an electronegative gas and the detailed reactions are described in Part D.

2. Vibrational, rotational, and excitation temperature measurements

The vibrational temperature T_{vib} is measured from the emission spectrum of the N_2 second positive band ($C^3\Pi_u \rightarrow B^3\Pi_g$). Four vibrational bands, $\Delta\nu = 1$(1-0,2-1,3-2), $\Delta\nu = -1$(0-1,1-2,2-3), $\Delta\nu = -2$(0-2,1-3,2-4), and $\Delta\nu = -3$(0-3, 1-4,2-5) are used to estimate T_{vib} based on the Boltzmann-plot

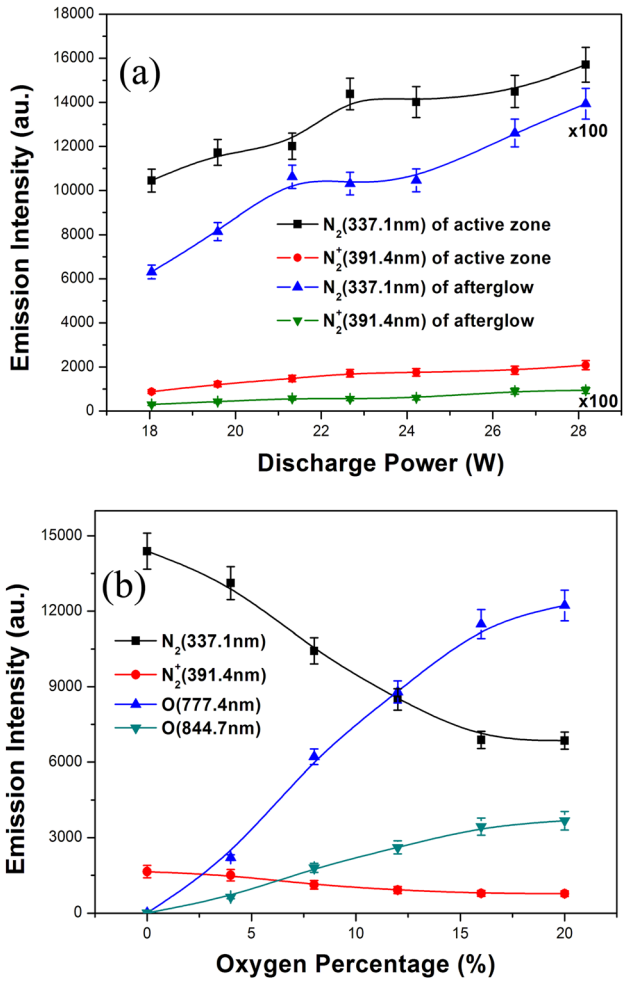

FIG. 5. Emission intensities of the main lines in the active region of the nitrogen discharge (a) at a flow rate 1000 l/h and nitrogen/oxygen discharge (b) at a flow rate 1000 l/h, discharge power 22.7 W.

method.[32] Fig. 6 shows a typical Boltzmann-plot of the relative intensity distributions. After taking into account the scattered data points and fitting errors, the vibrational temperature obtained from Fig. 6 is estimated to be about (3933 ± 400) K. The rotational structures of the nitrogen C-B (0-2) band between 368 and 381 nm are used to determine the gas temperature (T_g) by assuming that the gas temperature is equal to the rotational temperature. The spectrum is calculated by Specair software.[24] As shown in Fig. 7(a), the best fit is obtained at a rotational temperature of (1650 ± 50) K in the active region characterized by a small flow rate of 250 l/h and a temperature higher than the melting point of copper. The time-averaged spectra from the afterglow in Fig. 7(b) suggests a rotational temperature of (330 ± 50) K at a flow rate of 1000 L/h indicating that the plasma can be touched by hands.

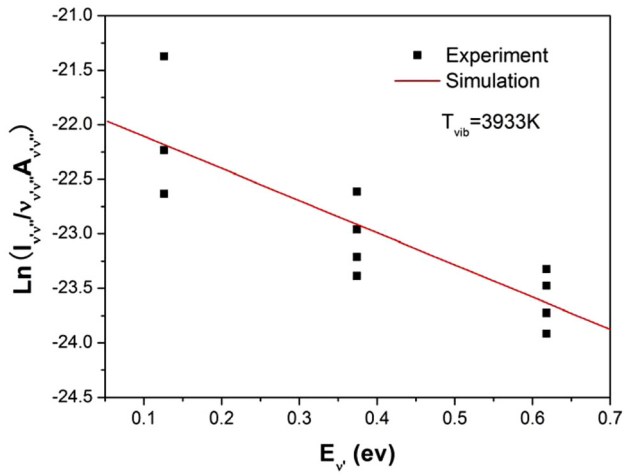

FIG. 6. Typical Boltzmann plot of the N_2 vibrational distribution.

Fig. 4(a) shows cooper emission lines at 324.7 nm, 327.4 nm, 510.5 nm, 515.3 nm, and 521.8 nm and suggests that the materials are sputtered from the electrodes and excited by the plasma. The two-line method is utilized to determine the excitation temperature assuming that the distribution of atoms and ions in the different excited states have the Boltzmann distribution.[33,34] The parameters of the typical Cu I emission lines mentioned above are shown in Table I. In order to minimize the error, lines of approximately equal intensity are suggested.[36] In our experiments, the emission lines of 510.5 and 521.8 nm are used to estimate the excitation temperature T_{exc}. Considering the two lines emitted by an excited copper atom, the excitation temperature can be calculated by the following equation:[37]

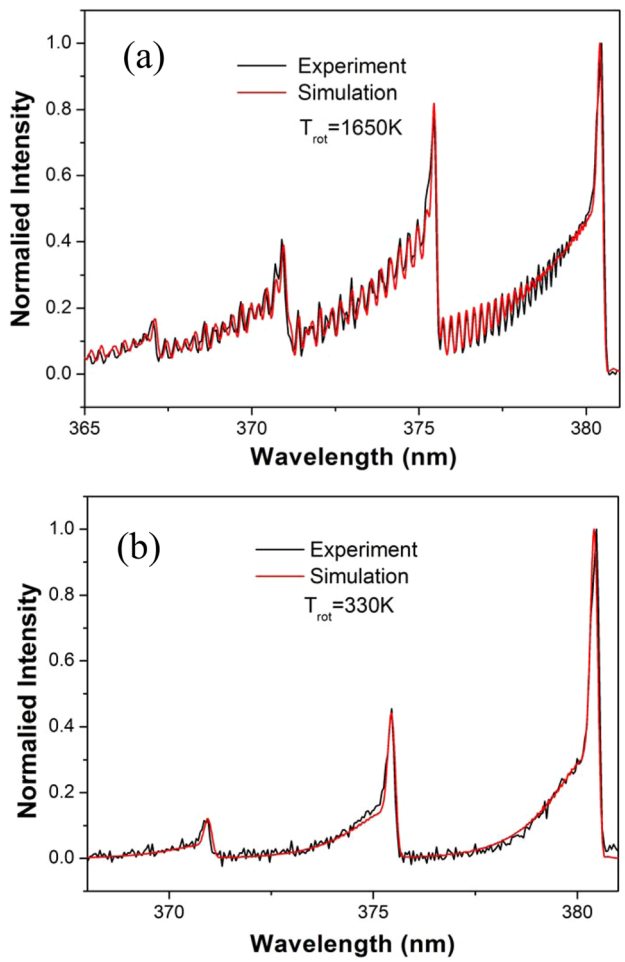

FIG. 7. Experimental and simulated spectra of the Nitrogen C-B(0-2) in nitrogen discharge at a discharge power of 22.7 W: (a) Active region at a flow rate 250 l/h and (b) Afterglow at a flow rate of 1000 l/h and 5 mm away from the nozzle.

TABLE I. Line parameters of the Cu I lines.[35]

Line	λ (nm)	E_i (eV)	E_j (eV)	g_i	g_j	A_{ij} (10^{-8}s^{-1})
Cu I	324.754	3.817	0	4	2	1.37
Cu I	327.396	3.786	0	2	2	1.36
Cu I	510.554	3.817	1.389	4	6	0.02
Cu I	515.324	6.191	3.786	4	2	0.60
Cu I	521.820	6.192	3.817	6	4	0.75

$$T_{exc} = \frac{E_2 - E_1}{k_B}\left[\ln\left(\frac{I_1\lambda_1 g_2 A_2}{I_2\lambda_2 g_1 A_1}\right)\right]^{-1}, \quad (1)$$

where E_2 and E_1 are the excitation potential levels of the related lines, k_B is Boltzman's constant, I is the line transition intensity, λ is the wavelength, g is the statistical weight, and A is the emission constant.

Fig. 8 presents the rotational, vibrational, and excitation temperature of the active and afterglow region measured from the N_2 and N_2/O_2 discharges as a function of the discharge power, gas flow rate, oxygen percentage, and distance from the nozzle. The trend of $T_{exc} > T_{vib} > T_{rot}$ is revealed in Fig. 8 regardless of the experimental conditions and therefore, the plasma source operates under non-equilibrium conditions. As shown in Figs. 9(a) and 9(b), these three types of temperature (T_{exc}, T_{vib}, and T_{rot}) in the afterglow are lower than those in the active region and it is because the plasma can obtain the sustained energy in the active region but not in the afterglow region as the electric field exists in the active region. Compared to the trends of T_{vib} and T_{rot}, there is no obvious change in T_{exc} under different experimental conditions. Besides, the excitation temperature measured by the two-line method may be lower than that calculated by the Boltzmann method based on several excited Ar emission lines. This is because the excitation temperature can be obtained from the upper excited state distribution, which corresponds to a portion of the electrons in the energy distribution function.[38] T_{vib} and T_{rot} increase with the discharge power and oxygen percentage but decrease with the flow rate and the distance from the nozzle. Since collisions among particles increase with the flow rate, more particles will participate in the energy exchange. Therefore, the rotational temperature and vibrational temperature will decrease[39] and similar results have been reported.[40–42] Fig. 8(c) shows that the rotational and vibrational temperature in the active region increases by about 800 K and 2000 K, respectively, when the concentration of O_2 goes up from 0% to 20%. The heating effect may be explained by the more effective energy

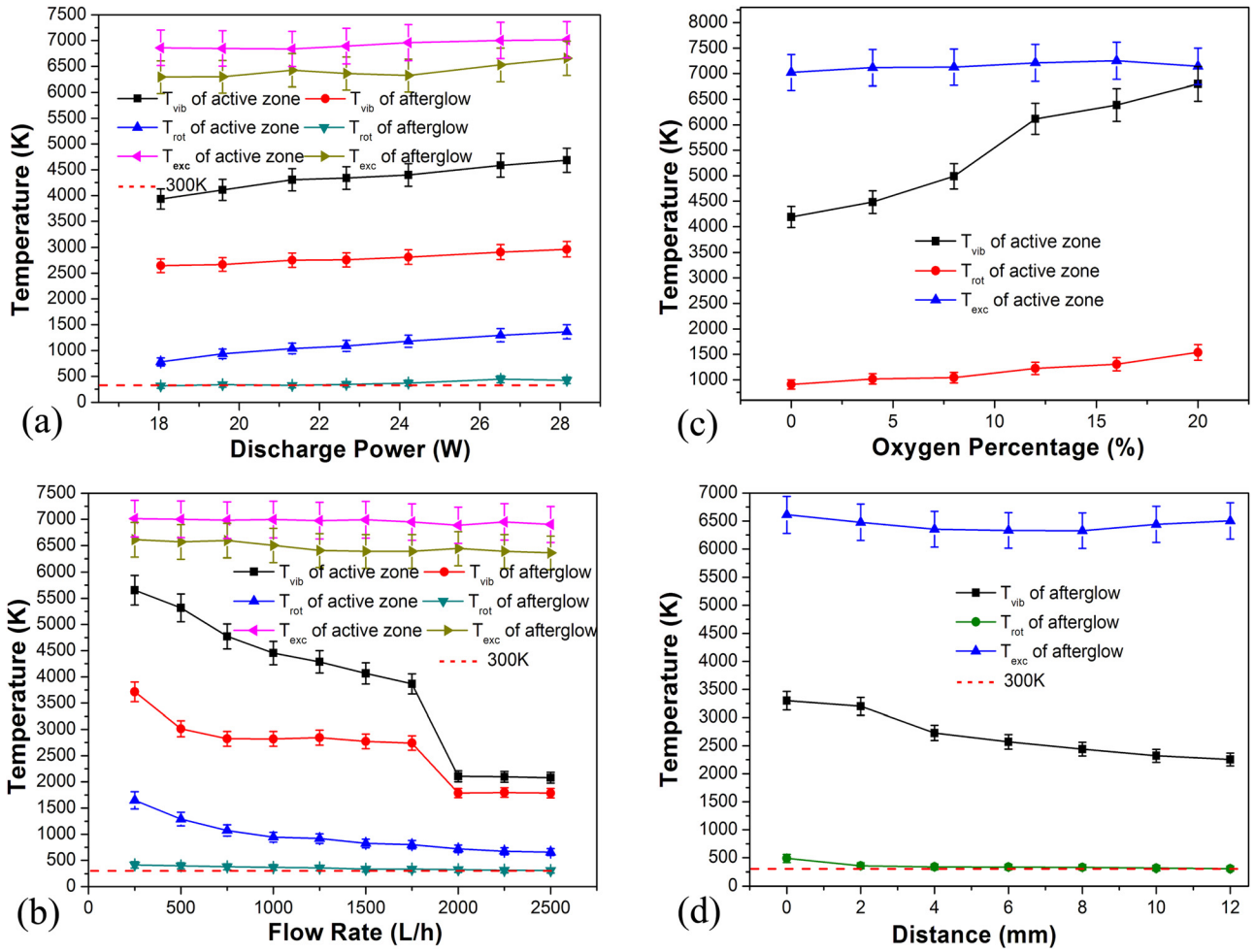

FIG. 8. Vibrational, rotational, and excitation temperature in the active region and afterglow 5 mm away from the nozzle: (a) Discharge at a flow rate of 1000 l/h in nitrogen; (b) Discharge power of 22.7 W in nitrogen; (c) Discharge power of 22.7 W and flow rate of 1000 l/h; (d) Discharge power of 22.7 W and flow rate of 1000 l/h in nitrogen.

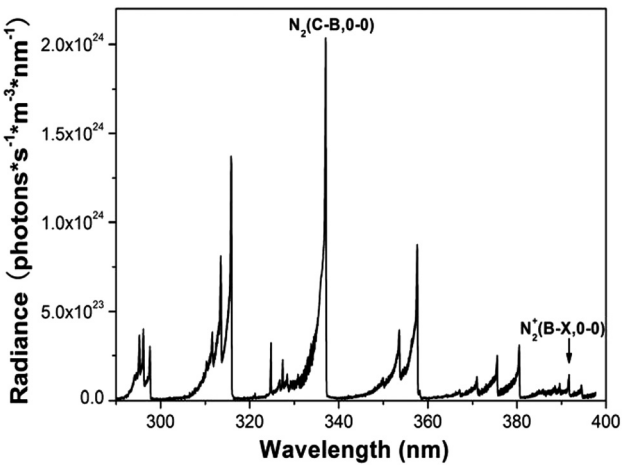

FIG. 9. Irradiance intensity spectra in the nitrogen discharge.

transfer from electrons to molecular O_2 *via* excitation of vibrational and rotational levels of oxygen. The process heats the gas due to the effective energy relaxation processes in the presence of O_2 (Ref. 28) and can be verified by the decrease in the excitation temperature as shown in Fig. 8(c). In the afterglow region, T_{vib} and T_{rot} decrease with the distance from the nozzle as shown in Fig. 8(d). Because the plasma cannot obtain the sustained energy in this region, the energy diminishes due to collisions.

D. Electron density

The OES and numerical simulation of the nitrogen-containing plasma is carried out to determine the electron density in addition to the gas temperature of the plasma. In the active region of the plasma, nitrogen emission N_2(C–B), N_2^+(B–X), and N_2(B-A)) can be excited by direct or step-wise electron impact (2)–(8) as shown in the following:

$$N_2(X^1\Sigma_g^+) + e \rightarrow N_2(C^3\Pi_u) + e, \quad (2)$$

$$N_2(X^1\Sigma_g^+) + e \rightarrow N_2(A^3\Sigma_u^+) + e, \quad (3)$$

$$N_2(A^3\Sigma_u^+) + e \rightarrow N_2(C^3\Pi_u) + e, \quad (4)$$

$$N_2(A^3\Pi_u^+) + e \rightarrow N_2(B^3\Pi_g) + e, \quad (5)$$

$$N_2(X^1\Sigma_g^+) + e \rightarrow N_2^+(B^2\Sigma_u^+) + 2e, \quad (6)$$

$$N_2(A^3\Sigma_u^+) + e \rightarrow N_2^+(X^2\Sigma_g^+) + 2e, \quad (7)$$

$$N_2^+(X^2\Sigma_g^+) + e \rightarrow N_2^+(B^2\Sigma_u^+) + e. \quad (8)$$

Besides direct electron impact excitation, the excited states $N_2(B^3\Pi_g)$ and $N_2(C^3\Pi_u)$ can be partially populated by the pooling reaction of the metastable state $N_2(A^3\Sigma_u^+)$

$$N_2(A^3\Sigma_u^+) + N_2(A^3\Sigma_u^+) \rightarrow N_2(C^3\Pi_u, B^3\Pi_g) + N_2(X^1\Sigma_g^+). \quad (9)$$

N_2(C–B) and N_2^+(B–X) can be excited by direct electron impact excitation of the ground state neutral nitrogen molecule $N_2(X^1\Sigma_g^+)$ (2) and (6) as well as by stepwise excitation *via* the neutral metastable state $N_2(A^3\Sigma_u^+)$ (4) and ground state molecular ion $N_2^+(X^2\Sigma_g^+)$ (8), respectively. Considering the high rate constant of the pooling reaction (9) and stability of the molecules and atoms, more nitrogen molecules are in the ground state and so we mainly consider the direct electron impact for N_2(C). For N_2^+(B), since the nitrogen molecular ions are in the ground state (N_2^+(X)), step-wise electron impact from N_2^+(X) to N_2^+(B) needs to be considered.

The radiance intensity of N_2(C-B,0-0) and N_2^+(B-X,0-0) is used to estimate the electron density as follows:

$$I_{N_2}(C-B,0-0) = Q_{N_2(C)} \cdot N_{N_2} \cdot k_{N_2(C)} \cdot V_{plasma} \cdot n_e, \quad (10)$$

$$I_{N_2^+}(B-X,0-0) = Q_{N_2^+(B)} \cdot (N_{N_2} \cdot k_{N_2^+(B)} + N_{N_2^+(X)} \cdot k^+_{N_2^+(B)}) \times V_{plasma} \cdot n_e, \quad (11)$$

where $Q_{N_2(C)}$ and $Q_{N_2^+(B)}$ are the weight for N_2(C-B,0-0) and N_2^+(B-X,0-0), which can be found from other papers,[43–47] N_{N_2} is the density of N_2 at the gas temperature, $N_{N_2^+(X)}$ is the density of nitrogen molecular ions in the ground state, $k_{N_2(C)}$ and $k_{N_2^+(B)}$ are the rate constants of N_2 (C–B) and N_2^+(B–X) for direct electron impact excitation from the ground state N_2(X), respectively, $k^+_{N_2^+(B)}$ is the rate constant of N_2^+(B–X) for electron impact excitation from $N_2^+(X^2\Sigma_g^+)$, V_{plasma} is the volume of the plasma in the active region, and n_e is the electron density. The excitation rate constants by electron impact $k_{N_2(C)}$, $k_{N_2^+(B)}$, and $k^+_{N_2^+(B)}$ depend on EEDF ($f_v(E)$) and the excitation cross section σ_{exc} is as follows:

$$k_{exc} = 4\pi\sqrt{2}\int_0^\infty f_v(E)\sqrt{\frac{2e}{m}}E \cdot \sigma_{exc}(E)dE, \quad (12)$$

where m and e are the electron mass and elementary charge of electron, respectively, and E is the kinetic energy of electrons (in eV). $f_v(E)$ is normalized to satisfy the following relationship:

$$4\pi\sqrt{2}\int_0^\infty f_v(E)dE = 1. \quad (13)$$

To calculate these rate constants, we set the pressure at 1 atm and the corresponding frequency in the discharge, and the program code BOLSIG+ is adopted by solving the electron Boltzmann equation (BE) to obtain the electron transport coefficients and rate coefficients.[48] Apart the aforementioned main electronic state excitations (2–9), the vibrational, rotational, and other electronic state excitations excited by direct electron impact from the ground state of the nitrogen molecules are considered in the calculation and the electron impact cross section data can be found from Refs. 49 and 50. Here, it is assumed that the number of N_2^+ in the high electronic state is much smaller than that in the ground state. The plasma is quasi-neutral and the electron density is assumed to be approximately equal to the density of $N_2^+(X^2\Sigma_g^+)$. Functions (10) and (11) can be transformed to (14) and (15) as follows:

TABLE II. Reactions considered in the calculation. (Note: $O_2(M)$ is the momentum process, $O_2(X,r)$ and $O_2(X,v'=1–4)$ are rotational and vibrational excitations, respectively. All the cross data of the excitations can be found from Ref. 49.)

No.	Reaction	No.	Reaction
17	$O_2(X)O_2(X)(M)$	24	$O_2(X)+e\rightarrow O_2(8.4eV)+e$
18	$O_2(X)+e\rightarrow O_2(X,r)+e$	25	$O_2(X)+e\rightarrow O_2(9.97eV)+e$
19	$O_2(X,v'=0)+e\rightarrow O_2(X,v'=1-4)+e$	26	$O_2(X)+e\rightarrow 2O+e$
20	$O_2(X)+e\rightarrow O_2(X,a^1\Delta)+e$	27	$O_2(X)+e\rightarrow O_2^+ +2e$
21	$O_2(X)+e\rightarrow O_2(X,b^1\Sigma)+e$	28	$2O_2(X)+e\rightarrow O_2(X)+O_2^-$
22	$O_2(X)+e\rightarrow O_2(4.5eV)+e$	29	$O_2(X)+e\rightarrow O^- +O$
23	$O_2(X)+e\rightarrow O_2(6.0eV)+e$		

$$n_e=\frac{I_{N_2}(C-B,0-0)}{Q_{N_2(C)}\cdot N_{N_2}\cdot k_{N_2(C)}\cdot V_{plasma}}. \tag{14}$$

$$n_e=\frac{\frac{I_{N_2^+}(B-X,0-0)}{I_{N_2}(C-B,0-0)}\cdot Q_{N_2(C)}\cdot N_{N_2}\cdot k_{N_2(C)}-Q_{N_2^+(B)}\cdot N_{N_2}\cdot k_{N_2^+(B)}}{Q_{N_2^+(X)}\cdot k^+_{N_2(B)}}. \tag{15}$$

We include the function between n_e and current density j as shown in the following:

$$n_e=\frac{j}{e\upsilon_d}, \tag{16}$$

where υ_d is the drift velocity of the electrons, which can also be obtained by the program code BOLSIG+ by solving the electron Boltzmann equation. When oxygen is added to nitrogen, the discharge becomes more complex and hence we consider direct electron impact for oxygen by including the 17 processes listed in Table II in the calculation.

Fig. 9 presents the absolute radiance intensity of the emission spectra for the vibrational band N_2(C-B) and N_2^+(B-X) in the nitrogen discharge. The value of the axis is the corresponding photons density after computation with consideration of the plasma volume in active region. Because k_{exc} is calculated for the variable electric field E by solving the electron Boltzmann equation and n_e versus E is obtained. By applying functions (14)–(16), we obtain the average electron density distribution in a wide range of electric field E. Owing to the inaccuracy in the measured values and applied rate constants arising from the uncertainty in the cross data, the intersection of the three curves is not a single point and three points are shown in the inset of Fig. 10. Although there are three intersections, they are very close and the average value is used to estimate the electron density. According to Fig. 10, n_e is approximately equal to $4.2\times10^{20}/m^3$ and the electric field E is about 10^6 V/m at a flow rate of 1000 l/h and discharge power of 22.7 W in nitrogen.

As shown in Fig. 11, the electron density increases from $3.0\times10^{20}/m^3$ to $5.6\times10^{20}/m^3$ when the discharge power goes up from 18 to 28 W. However, as shown in Fig. 12, the electron density shows very few changes at a fixed discharge power when the flow rate increases and it is almost flat at $4.2\times10^{20}/m^3$. It indicates that the electron density is affected by the discharge power more than the flow rate. Because the discharge power increases, more power is dissipated into the plasma and the radiance intensity increases. The electron density decreases but nonetheless, when the discharge power is fixed, the power dissipated to the plasma may only change slightly even if the flow rate changes substantially and hence the electron density does not change significantly. While oxygen is added to nitrogen, there is an apparent drop in the electron density a shown in Fig. 13. Since oxygen is an electronegative gas which has a lower threshold energy of the excitation levels than nitrogen, some

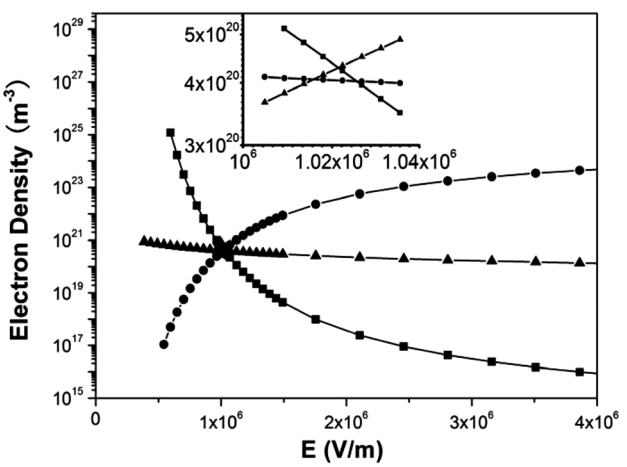

FIG. 10. Electron density calculated by applying functions (14—■—), (15—●—), and (16—▲—) in a wide range of electric field E.

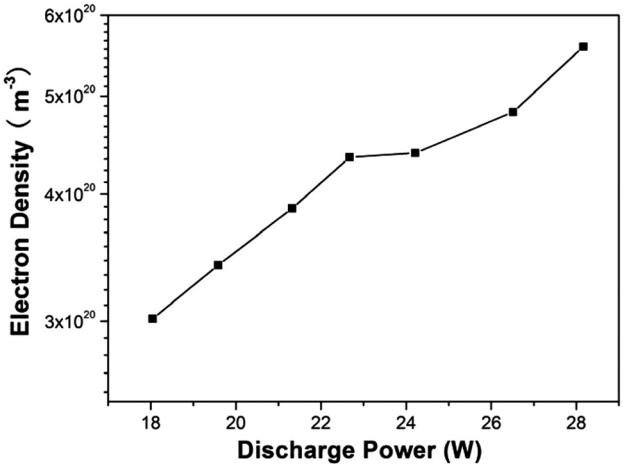

FIG. 11. Relationship between the electron density and discharge power at a flow rate of 1000 l/h.

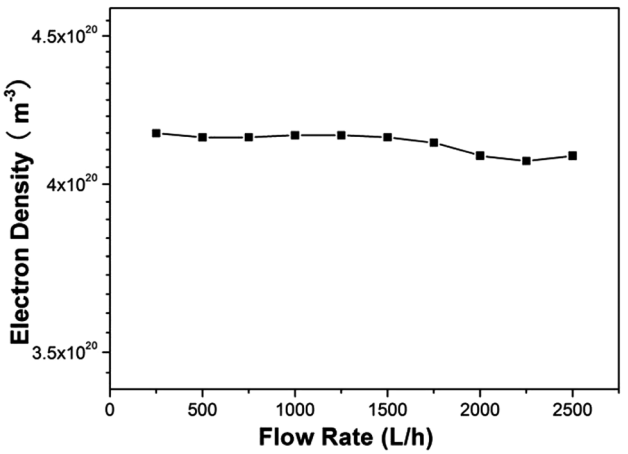

FIG. 12. Relationship between the electron density and flow rate at a discharge power of 22.7 W.

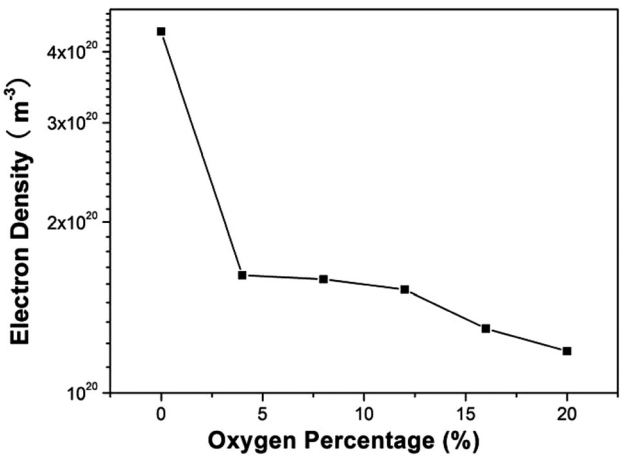

FIG. 13. Relationship between the electron density and oxygen percentage at a discharge power of 22.7 W and flow rate of 1000 l/h.

discharge power is used to excite oxygen and some electrons are consumed according to the three body attachment function (28) in Table II because the ground state of O_2^- is more stable.[51] Consequently, there is a sharp drop in the electron density when oxygen is mixed with nitrogen. With the oxygen percentage increases from 4% to 20%, the electron density decreases from $1.6 \times 10^{20}/m^3$ to $1.1 \times 10^{20}/m^3$.

IV. CONCLUSION

An atmospheric-pressure non-thermal plasma jet operating on N_2 and N_2/O_2 is evaluated systematically. The length of plasma jet increases with the discharge power and gas flow rate but decreases with the oxygen concentration. It does not change significantly when the discharge frequencies are varied. The plasma parameters such as the excited species, rotational temperature, vibrational temperature, and excitation temperature in different discharge conditions are determined by OES. The trend of $T_{exc} > T_{vib} > T_{rot}$ is observed irrespective of experimental conditions, indicating that the plasma is far from thermal equilibrium. T_{vib} and T_{rot} increase with the discharge power and oxygen concentration but decrease with the gas flow rate and distance from the nozzle. The radiance intensities of N_2(C-B,0-0) and N_2^+(B-X,0-0) are used to estimate the electron density in the nitrogen as well as nitrogen/oxygen discharge. The electron density increases from $3.0 \times 10^{20}/m^3$ to $5.6 \times 10^{20}/m^3$ as the discharge power increases from 18 to 28 W and has a value of $4.2 \times 10^{20}/m^3$ when the flow rate is changed while the discharge power is fixed. Addition of oxygen decreases the electron density from $4.2 \times 10^{20}/m^3$ to $1.6 \times 10^{20}/m^3$ and when more oxygen is added, the electron density diminishes smoothly.

ACKNOWLEDGMENTS

This work was jointly supported by the National Natural Science Foundation of China under Grant No. 11005126, Hefei Institute of Physical Science, Chinese Academy of Sciences (CASHIPS) Dean Fund No. YZJJ201331, as well as City University of Hong Kong Applied Research Grant (ARG) No. 9667069. We would like to thank Christophe Laux for fruitful discussion on the synthetic spectra.

[1]M. Laroussi and T. Akan, Plasma Process. Polym. **4**, 777 (2007).
[2]X. Lu, M. Laroussi, and V. Puech, Plasma Sources Sci. Technol. **21**, 034005 (2012).
[3]C. Tendero, C. Tixier, P. Tristant, J. Desmaison, and P. Leprince, Spectrochimi. Acta, Part B **61**, 2 (2006).
[4]C. Cheng, P. Liu, L. Xu, L. Y. Zhang, R. J. Zhan, and W. R. Zhang, Chin. Phys. **15**, 1544 (2006).
[5]M. H. Han, J. H. Noh, T. I. Lee, J. H. Choi, K. W. Park, H. S. Hwang, K. M. Song, and H. K. Baik, Plasma Process. Polym. **5**, 861 (2008).
[6]M. Laroussi, Plasma Process. Polym. **2**, 391 (2005).
[7]H. S. Uhm, S. C. Cho, Y. C. Hong, Y. G. Park, and J. S. Park, Appl. Phys. Lett. **92**, 071503 (2008).
[8]C. Cheng, L. Y. Zhang, and R. J. Zhan, Surf. Coat. Technol. **200**, 6659 (2006).
[9]C. M. Du, J. H. Yan, and B. G. Cheron, Plasma Chem. Plasma Process. **27**, 635 (2007).
[10]P. Zhao, W. Zheng, Y. D. Meng, and M. Nagatsu, J. Appl. Phys. **113**, 123301 (2013).
[11]G. Fridman, A. D. Brooks, M. Balasubramanian, A. Fridman, A. Gutsol, V. N. Vasilets, H. Ayan, and G. Friedman, Plasma Process. Polym. **4**, 370 (2007).
[12]S. Deng, C. Cheng, G. Ni, Y. Meng, and H. Chen, Jpn. J. Appl. Phys., Part 1 **47**, 7009 (2008).
[13]S. Deng, C. Cheng, G. Ni, Y. Meng, and H. Chen, Curr. Appl. Phys. **10**, 1164 (2010).
[14]J. Shen, C. Cheng, S. D. Fang, H. B. Xie, Y. Lan, G. H. Ni, Y. D. Meng, J. R. Luo, and X. K. Wang, Appl. Phys. Exp. **5**, 036201 (2012).
[15]Y. C. Hong, W. S. Kang, Y. B. Hong, W. J. Yi, and H. S. Uhm, Phys. Plasmas **16**, 123502 (2009).
[16]Y. C. Hong and H. S. Uhm, Appl. Phys. Lett. **89**, 221504 (2006).
[17]J. F. Kolb, A. A. H. Mohamed, R. O. Price, R. J. Swanson, A. Bowman, R. L. Chiavarini, M. Stacey, and K. H. Schoenbach, Appl. Phys. Lett. **92**, 241501 (2008).
[18]S. Djurovic, M. Cirisan, A. V. Demura, G. V. Demchenko, D. Nikolic, M. A. Gigosos, and M. A. Gonzalez, Phys. Rev. E **79**, 046402 (2009).
[19]N. Konjević, M. Ivković, and N. Sakan, Spectrochim. Acta, Part B **76**, 16 (2012).
[20]J.-Y. Choi, N. Takano, K. Urabe, and K. Tachibana, Plasma Sources Sci. Technol. **18**, 035013 (2009).
[21]F. Leipold, R. H. Stark, A. El-Habachi, and K. H. Schoenbach, J. Phys. D:Appl. Phys. **33**, 2268 (2000).
[22]K. Muraoka and A. Kono, J. Phys. D: Appl. Phys. **44**, 043001 (2011).
[23]L. Prevosto, H. Kelly, and B. R. Mancinelli, J. Appl. Phys. **112**, 063302 (2012).
[24]C. O. Laux, T. G. Spence, C. H. Kruger, and R. N. Zare, Plasma Sources Sci. Technol. **12**, 125 (2003).

[25]S. Keller, P. Rajasekaran, N. Bibinov, and P. Awakowicz, J. Phys. D: Appl. Phys. **45**, 125202 (2012).
[26]P. Rajasekaran, N. Bibinov, and P. Awakowicz, Meas. Sci. Technol. **23**, 085605 (2012).
[27]P. Rajasekaran, C. Ruhrmann, N. Bibinov, and P. Awakowicz, J. Phys. D: Appl. Phys. **44**, 485205 (2011).
[28]X. L. Deng, A. Y. Nikiforov, P. Vanraes, and C. Leys, J. Appl. Phys. **113**, 023305 (2013).
[29]J. L. Walsh and M. G. Kong, Appl. Phys. Lett. **99**, 081501 (2011).
[30]G. D. Stancu, F. Kaddouri, D. A. Lacoste, and C. O. Laux, J. Phys. D: Appl. Phys. **43**, 124002 (2010).
[31]Y. Xian, X. Lu, S. Wu, P. K. Chu, and Y. Pan, Appl. Phys. Lett. **100**, 123702 (2012).
[32]G. Herzberg, *Molecular Spectra and Molecular Structure I. Spectra of Diatomic Molecules* (Van Nostrand, Princeton, 1953) (in Chinese).
[33]Y. D. Hoyer, B. N. Sismanoglu, and K. G. Grigorov, Eur. Phys. J. D **66**, 171 (2012).
[34]B. N. Sismanoglu, K. G. Grigorov, R. Caetano, M. V. O. Rezende, and Y. D. Hoyer, Eur. Phys. J. D **60**, 505 (2010).
[35]See http://physics.nist.gov/PhysRefData/Handbook/Tables/coppertable3.htm for Persistent Lines of Neutral Copper (Cu I).
[36]A. Nekahi, M. Farzaneh, C. Volat, and W. A. Chisholm, in *IEEE Conference on Electrical Insulation and Dielectric Phenomena, Quebec City, Canada* (2008).
[37]H. R. Griem, *Principles of Plasma Spectroscopy* (Cambridge University Press, 1997).
[38]B. N. Sismanoglu, J. Amorim, J. A. Souza-Corrêa, C. Oliveira, and M. P. Gomes, Spectrochim. Acta, Part B **64**, 1287 (2009).
[39]C. Biloiu, X. Sun, Z. Harvey, and E. Scime, Rev. Sci. Instrum. **77**, 10F117 (2006).
[40]B. Hrycak, M. Jasiński, and J. Mizeraczyk, J. Phys.: Conf. Ser. **406**, 012037 (2012).
[41]Y. Uchida, K. Takaki, K. Urashima, and J. S. Chang, IEEE Trans. Dielectr. Electr. Insul. **11**, 491 (2004).
[42]P. Jamróz, W. Żyrnicki, and P. Pohl, Spectrochim. Acta, Part B **73**, 26 (2012).
[43]N. Bibinov, N. Knake, H. Bahre, P. Awakowicz, and V. Schulz-von der Gathen, J. Phys. D: Appl. Phys. **44**, 345204 (2011).
[44]S. Keller, N. Bibinov, A. Neugebauer, and P. Awakowicz, J. Phys. D: Appl. Phys. **46**, 025402 (2013).
[45]R. Pothiraja, N. Bibinov, and P. Awakowicz, J. Phys. D: Appl. Phys. **43**, 495201 (2010).
[46]S. V. Pancheshnyi, S. M. Starikovskaia, and A. Y. Starikovskii, Chem. Phys. Lett. **294**, 523 (1998).
[47]S. V. Pancheshnyi, S. M. Starikovskaia, and A. Y. Starikovskii, Chem. Phys. **262**, 349 (2000).
[48]G. J. M. Hagelaar and L. C. Pitchford, Plasma Sources Sci. Technol. **14**, 722 (2005).
[49]A. V. Phelps and L. C. Pitchford, Phys. Rev. A **31**, 2932 (1985).
[50]Y. Itikawa, J. Phys. Chem. Ref. Data **35**, 31 (2006).
[51]M. A. Lieberman and A. J. Lichtenberg, *Principles of Plasma Discharges and Materials Processing*, 2rd ed. (John Wiley & Sons, Inc. 2005).